MICROSTRUCTURE, CELL-TO-CELL COUPLING AND ION CURRENTS AS DETERMINANTS OF ELECTRICAL PROPAGATION AND ARRHYTHMOGENESIS

Jan P. Kucera[ξ], MD

Stephan Rohr[ξ], MD,

André G. Kléber, MD[‡],

From the Department of Physiology, University of Bern, Bern, Switzerland[ξ] and the Department of Pathology, Harvard Medical School, Boston, MA[‡]

RUNNING TITLE: DETERMINANTS OF CARDIAC ELECTRICAL PROPAGATION

Journal Subject Terms: Electrophysiology, Arrhythmias, Basic Science, Research, Animal Models of Human Disease

Key Words: Experimental Models, Electrical Propagation, Safety of Propagation, Excitation, Cell-to-Cell Coupling, Ion Channels, Fiber Architecture, Fibroblasts

Address for correspondence:

André G. Kléber, MD
Department of Pathology, Harvard Medical School
Beth Israel Deaconess Medical Center, DANA 714
330 Brookline Avenue
Boston, MA 02215
phone: 617-667-4346
fax: 617-667-2943
e-mail: akleber@bidmc.harvard.edu

INTRODUCTION

Rapid electrical impulse spread from the sino-atrial node to the atria, the atrio-ventricular node and the ventricles is prerequisite for coordinated cardiac contraction. In cardiac arrhythmias, disturbed impulse spread can lead to ventricular or atrial tachycardia, fibrillation and sudden cardiac death.

A change in electrical impulse propagation had already been proposed to underlie re-entrant arrhythmias at the beginning of the 20th century. [1] Slowing of propagation and the formation of unidirectional propagation block represent the two most important changes leading to circulating and re-entrant propagation. Unidirectional propagation block is the prerequisite for the wavefront to reenter non-refractory tissue of the original propagation path. Knowledge of the mechanisms governing abnormal impulse propagation and formation of propagation block at the level of cellular networks is important for our understanding of arrhythmogenesis and the principles underlying electrical and drug therapy. This article reviews experimental work and modeling studies carried out to understand the basic mechanisms of cardiac impulse propagation, with specific emphasis laid on the relation between propagation and cardiac microstructure. Normally, layers and strands of electrically coupled myocytes separated by connective tissue create a mostly anisotropic compartmentation in atrial and ventricular myocardium. However, compartmentalization can assume pathological forms when fibrosis is enhanced with increasing age and during reparative fibrosis in pathological settings (myocardial infarction, volume/pressure overload, some forms of hereditary diseases). Although structural heterogeneities favor the formation of re-entrant circuits, spiral waves occur in tissues with homogeneous electrical and structural properties on the basis of time-dependent local changes in refractoriness, which set up the scenario for unidirectional block formation. [2]

The selected references cited in this short review cannot cover the large body of published literature. Moreover, this article will cover neither the topic of spiral waves nor early and delayed afterdepolarizations (disturbed Ca^{2+} cycling), which play a major role in the initiation of cardiac arrhythmias.

CONTINUOUS ELECTRICAL PROPAGATION IN CARDIAC CELL STRANDS: EFFECT OF DEPOLARIZING ION CURRENTS AND CELL-TO-CELL COUPLING

Basic Mechanism of Impulse Propagation and the Concept of Propagation Safety

Historically, a simple model of cardiac impulse propagation was derived by drawing an analogy between a cardiac muscular trabecula, Purkinje fibers and a non-myelinated nerves as cylindrically shaped excitable structures. In these models, the extracellular space is separated from the intracellular space by the excitable surface membrane of the cylinder. [3] The simplified intracellular space lumps the cytoplasm of the cells and the cell-to-cell junctions into a single resistive compartment. With the advent of computer simulations and high resolution optical mapping technology, more detailed models of cardiac tissue were established, [4, 5]. It became possible to define the role of gap junction channels in electrical cardiac propagation experimentally, and to compute the contribution of ion and gap junction channels to propagation. [6, 7] The model depicted in Figure 1 A shows a simple chain of cardiomyocytes interconnected by electrical resistors representing gap junction channels. Impulse propagation in this model is driven by upstream excitation of cardiac cells producing depolarizing current flowing axially into the downstream cells. This current, provided it is large enough, excites the downstream cells, which in turn deliver axial current to further downstream excitable elements. Accordingly, the wave front separating excited (upstream) from not-excited (downstream) tissue propagates along the cell chain. As mentioned above, slow conduction and conduction block are major determinants for the initiation of reentrant excitation. Therefore, besides understanding what factors determine conduction velocity, an important question is how **safe** action potential propagation is under normal and pathological conditions. Shaw and Rudy provided a comprehensive approach to the computation of this so-called safety factor (SF), as illustrated in Figure 1B, and as formulated in equation 1: [6]

equation 1 ……

$$SF = \frac{\int_A I_C dt + \int_A I_{OUT} dt}{\int_A I_{IN} dt}$$

The denominator of this equation corresponds to the electrical charge flowing from upstream into a given cell during excitation (Figure 1B, blue). The first term of the numerator refers to the capacitive charge forming the upstroke of the action potential (red), and the second term to the charge flowing downstream out of the cell (green) to excite the downstream cells and propagate the action potential. The integration range A is defined as the time window during which the membrane is being depolarized. [6] Intuitively, this definition is straightforward: propagation is safe (SF >1), if the denominator is smaller than the numerator, i.e., if the axial (or so-called *electrotonic*) current required to *excite* a given downstream cell is smaller than the ion current *generated* by this same cell. Over the years several algorithms for describing the margin of safety of propagation have been proposed. [6, 8-10] While the definition given by equation 1 is very useful for understanding the general concept of propagation safety, algorithms describing propagation safety in multidimensional or discontinuous tissues are necessarily more complex. [9, 10]

The Effect of Depolarizing Ion Currents and Cell-to-cell Uncoupling on Impulse Propagation

In pathological settings, ion channel inhibition and cell-to-cell uncoupling are the main causes underlying cardiac propagation slowing.[7]

The effects of reducing the Na^+ current vs. electrical cell-to-cell coupling on SF and propagation velocity is illustrated in Figure 2 taken from a computational study of propagation in a chain of single myocytes.[6] There is a striking difference between the two effects, which is best explained by looking at the change in SF. Reducing Na^+ current leads to a monotonic decrease in SF with propagation block occurring at approximately 85% reduction of I_{Na}. Propagation velocity at which propagation block occurs is still relatively high, about 15 cm/s. Reducing cell-to-cell coupling increases SF markedly (up to about 2-fold). As a consequence, propagation becomes safer (more stable), and therefore, can decrease to very low values in the order of a centimeter per second before the SF drops abruptly and propagation block occurs.

In accordance with theoretical work, marked differences between the effects of Na^+ channel inhibition and decrease in cell-to-cell coupling on propagation have been reported in experimental studies. Figure 3A

illustrates propagation in engineered strands of neonatal rat cardiomyocytes in which tetrodotoxin has been added to inhibit inward Na^+ current (I_{Na}).[11] This inhibition led to propagation carried by the L-type slow inward Ca^{2+} current ($I_{Ca,L}$) at a velocity of 13 cm/s. In contrast to hearts of small rodents, inhibition of I_{Na} in large mammalian hearts by perfusion with elevated extracellular K^+ (partial Na^+ channel inactivation due to the elevation of resting membrane potential) produces propagation block in longitudinal direction of muscular fibers at 40cm/s and 20cm/s in transverse direction.[12] Slow propagation carried by $I_{Ca,L}$ at 12 cm/s is observed in these hearts after addition of norepinephrine.[12]

Propagation slowing due to cell-to-cell uncoupling is shown in Figure 3B. Experimentally, uncoupling was achieved by either adding an uncoupling agent (palmitoleic acid [11]) or by genetically ablating connexin43 (Cx43) in engineered fetal murine myocytes.[13] As illustrated in Figure 3B, genetic ablation of Cx43 leads to a reduction of intercellular electrical conductance (g_j,) by > 90% (the small remaining conductance being due to the presence of Cx45 [13, 14]), and to a decrease in propagation velocity to very slow values (2.1 cm/s).

The *increase of the safety of propagation* with cell-to-cell uncoupling is explained by a changed relation between the upstream source of axial current and the downstream sink: the increase in cell-to-cell resistance will, on the one hand, slows the charging of the membrane capacitance by axial current flow and consequently, cause slow propagation (Figures 1B and 2). On the other hand, it will decrease the downstream current sink (i.e., increase its impedance) and constrain the axial current to a smaller region downstream. This *protective* effect of increased downstream impedance has been recognized early on and was used to explain, for instance, why a small sino-atrial node can excite a large atrium**.** [15, 16]

THE EFFECT OF STRUCTURAL DISCONTINUITIES ON PROPAGATION: INTERACTION BETWEEN MICROSTRUCTURE, ION CURRENTS AND CELL-TO-CELL COUPLING

The mechanisms explained above can now be used to discuss the effect of the cardiac microstructure on propagation. This discussion is important because, as will be shown, the *discontinuous structure* is, besides intercellular coupling and depolarizing current flow, a third important determinant of cardiac propagation.

Both normal atrial and ventricular myocardium develop as discontinuous structures. Atria show large areas of trabeculation, ventricular myocardium shows a highly organized laminar structure with tissue layers that are 4-6 cells thick being wrapped around the left ventricular cavity.[17-19] These layers are tilted with respect to one another and connected by small muscular bridges (Figure 4A). Moreover, a network of muscular trabeculae outlines parts of the ventricular and atrial cavities. An increase of the amount of fibrous tissue separating muscle layers at a smaller scale is observed with increasing age, [20] in myocardial infarction and other diseases. [21]

Basic Rules Governing Discontinuous Cardiac Propagation

Experimental and theoretical work on discontinuous electrical propagation in the heart was pioneered by M.S. Spach and collaborators. [22-26] A result from an early experiment by is depicted in Figure 4B. [22] It shows that increasing fibrosis leads to heterogeneous impulse spread in atrial trabecula, a change that the same group later associated with microreentry in human atria. [26]

With the introduction of voltage-sensitive dyes to monitor action potentials from multiple sites at high resolution, it became possible to follow electrical excitation as it propagates across regions of discontinuous tissue geometries and to compare experimental findings with theoretical results obtained from computer modeling. [4, 9, 27] Impulse propagation in these basic geometrical patterns share common features characterized by a mismatch between the source (excited tissue) and the sink (resting tissue), which may consist in a single mismatch or in recurrent mismatches at small spatial intervals.

The main differences between continuous and discontinuous propagation relates to the fact that, in discontinuous propagation, the effects of depolarizing inward currents (I_{Na} and $I_{Ca,L}$) and cell-to-cell coupling become interdependent. The complex role of depolarizing ion currents in discontinuous cardiac structures has been recognized in experimental settings [28] and in theoretical work. [6, 29]

Figure 5Aa illustrates propagation from a narrow strand of cultured neonatal rat myocytes into a large bulk of tissue. [28] At the geometrical transition, the source-to-sink mismatch produces a local delay in the sequence of the action potential upstrokes indicating locally delayed propagation. In Figure 5Ab, the width of the narrow cell strand was reduced, which resulted in a larger source-to-sink mismatch that produced a local delay > 2ms. As

a consequence, excitation of the bulk tissue occurs at a time when the action potentials of the upstream strand have reached their peak. At this instant, a large part of Na^+ channels upstream is inactivated and $I_{Ca,L}$ flowing during the early action potential plateau becomes pivotal for eliciting action potentials downstream. Under these conditions, inhibitors of $I_{Ca,L}$ blocked propagation at the site of the source-to-sink mismatch. When the source-to-sink mismatch was made large enough to induce unidirectional conduction block, enhancers of $I_{Ca,L}$ rescued propagation (Figure 5Ac). The role of $I_{Ca,L}$ in discontinuous propagation has further been demonstrated in theoretical and experimental work describing action potential transfer between a cell pair, either an isolated myocyte and a virtual (simulated) myocytes connected by a resistor, or two simulated myocytes. [30, 31] Common to all of these experiments is the demonstration that local propagation delays shift the role of ion currents in the upstream driver cell(s) from a current with fast kinetics (I_{Na}) to a current with slower kinetics ($I_{Ca,L}$). In addition to $I_{Ca,L}$, transient outward current, I_{to}, can modulate propagation at sites of significant propagation delay. [32]

Similarly, electrical propagation at a site of source-to-sink mismatch is affected by the degree of local cell-to-cell coupling. [33, 34] This effect has been termed as paradoxical, [34] because, as shown in Figure 5B, partial uncoupling of tissue restores propagation at a site where a marked source-to-sink mismatch produced block in during normal cell-to-cell coupling. This suggests that cell-to-cell coupling has complex effects on conduction in tissues with discontinuous structures. [34] On the one hand, partial gap junctional uncoupling decreases propagation velocity, on the other hand it stabilizes propagation and may restore transmission of electrical impulses at the sites of block. These findings challenge the paradigm that drugs enhancing cell-to-cell coupling exert exclusively antiarrhythmic effects via an increase in propagation velocity as they may simultaneously precipitate unidirectional conduction blocks.

As shown in Figure 6, propagation across tissues with repetitive branches (branching tissue, such as found in infarct scars and, possibly, in the AV node) can be perceived as a process where a small source excites a large sink, and once excited, the large sink functions as the large source to excite a smaller downstream sink. Accordingly, this structure produces slow and, at the same time, safe conduction. In presence of elevated extracellular potassium, conduction velocities assume values in the range of a few centimeters per second thereby approaching values measured in uniform tissue structures during critical gap junctional uncoupling. [35]

The biophysical basis of the effect alternation of opposite mismatches as found in experiments has been defined in a theoretical study. [9]

Frequency Dependence of Propagation in Discontinuous Tissue

Frequency dependence of ion currents involved in the generation of the action potential has been known for several decades. In the case of the major depolarizing ion currents responsible for depolarization, I_{Na} and $I_{Ca,L}$, recovery from inactivation of the ion channels and availability for the next excitation cycle strongly depend on the membrane potential from which excitation emerges and on the resting membrane potential. [36, 37] While the dependence of depolarizing inward current and propagation velocity on resting membrane potential is complex and involves processes such as the dependence of membrane resistance on the transmembrane K^+ gradient and regulation of Na^+/K^+ pumping, [38, 39] it is undisputed that depolarization to levels more positive than about -65mV leads to marked reductions in Na^+ inward currents, conduction slowing, and eventually, frequency-dependent propagation block.

Importantly, source-to-sink mismatches, as caused by heterogeneities in tissue structure, *amplifies* the described frequency-dependence of propagation. [27, 40] Slowing of propagation across an expansion or an isthmus is not only dependent on the degree of structural heterogeneity, but also on the frequency of excitation. Figure 7A shows that stimulation of a strand of patterned neonatal ventricular myocytes which emerges into a bulk of cells (expansion) produces increasing local propagation delays ("Wenckebach-like" phenomenon) at the site of source-to-sink mismatch until propagation gets blocked after a certain number of beats. [40] This behavior (Figure 7B) is markedly enhanced with increasing source-to-sink mismatch. [27] A further factor related to frequency of excitation is the accumulation of intracellular Na^+ associated with increased rate.[40] Thus, excitation-dependent changes in intracellular ion composition will stimulate Na^+/K^+ pumping which shortens the action potential and prolongs the recovery time (diastolic interval). This effect increases excitability and restores propagation (Figure 7A),[40] These theoretical results have been verified by experimental findings. [40]

Frequency dependence of propagation in tissues with heterogeneous structure (fibrosis), are an important arrhythmogenic factor. Once an arrhythmia is initiated, and, cycle length is markedly shortened local propagation delays and blocks are expected to anchor to sites of source-to-sink mismatch in a manner dependent on the specific microstructure. Blocks at these locations are expected to be out of phase thus producing complex excitation patterns that change dynamically from beat-to-beat.

Propagation in cardiac tissue with heterogeneous connexin expression

A discontinuous conduction substrate can also arise at the cellular scale from the intercellular heterogeneity of bioelectrical properties. One important aspect of tissue inhomogeneity is heterogeneous gap junctional coupling. Such a situation may occur, e.g., due to intercellular differences in the sensitivity to acute ischemia, known to strongly alter gap junctional coupling. [41] Heterogeneous coupling can also arise from somatic mutations of connexin 43 (Cx43) leading to a genetic mosaicism of cardiac tissue known to be arrhythmogenic.[42] A contribution of heterogeneous cell-to-cell coupling to arrhythmogenesis has been postulated in heart failure patients. [43],[44] Experimentally, the situation of a strong heterogeneity of gap junctional coupling has been studied in the ventricles of wild-type/Cx43-knockout chimeric mice, in which heterogeneous proarrhythmic activation patterns were documented,[45] and in strands of co-cultured wild-type and Cx43-knockout murine ventricular myocytes.[14] In the latter preparations, conduction velocity assessed using optical mapping decreased with the proportion of Cx43-knockout cells and leveled off at a velocity of 2-3 cm/s that was supported by Cx45.[14] Further experiments conducted using microelectrode arrays[46] indicated that the relationship between velocity and Cx43-knockout cell proportion is nonlinear and that conduction in cell strands in which the two cellular genotypes are mixed is susceptible to block.

Insights into the mechanisms of conduction slowing and block were obtained from computer simulations using a detailed high-resolution model in which the cellular architecture of the tissue and the genotype of each cell were taken into account. [46] In tissue consisting of a random mixture of Cx43-knockout and wild-type cells, conduction was highly discontinuous with patches of myocytes being activated very rapidly while patch-to-patch activation was delayed. This heterogeneous pattern was caused by conduction through well-coupled myocytes meandering between irregularly positioned and poorly connected Cx43-knockout regions resulting

from the random arrangement of the two cell types. This led to increasingly large and very irregular current-to-load mismatches that slowed conduction and increased the probability of block. These results indicate that conduction in heterogeneous tissue is fundamentally different from conduction in idealized uniform tissue.

Source-to-sink mismatch and dispersion of local currents are associated with curved propagation wavefronts

As discussed above, structural obstacles (geometrical expansions, pivots points, isthmuses) produce curved wavefronts. Wavefront curvature is not only associated with a dispersion of local excitatory current and a mismatch between the upstream source and the downstream sink, but also with a change in the electrotonic interaction between excited and resting tissue. In contrast to a planar wave where excited tissue upstream of the wavefront is balanced by resting tissue downstream, the balance is tipped towards resting tissue in case of a convex wavefront. In this case, the electrical interaction between activated ion channels upstream and activated ion channels downstream is affected by the degree of curvature. Interaction between ion channels (I_{K1}, $I_{Ks,}$ I_{Kr} I_{Na}) is especially important for the behavior of the core and turning velocity of spiral waves. [47-49]

PRO-ARRHYTHMIC EFFECTS OF ELECTROTONIC CROSSTALK BETWEEN CARDIOMYOCYTES AND NON-CARDIOMYOCYTES

The possibility that stromal cells of the heart contribute to the generation of a pro-arrhythmic substrate by electrotonically interacting with parenchymal cells by means of gap junctional coupling is increasingly debated. Such interactions may be present between fibroblasts and cardiomyocytes in the healthy myocardium, between myofibroblasts (‘activated fibroblasts’) and cardiomyocytes at the border zone of healing infarcts, and, possibly, between stem or cardiac progenitor cells and cardiomyocytes following cell therapy.[50, 51] Moreover, electrical synchronization between donor and recipient atrial tissue following heart transplantation implicates functional electrical connection across fibroblasts. [52] Functional consequences of electrotonic crosstalk between non-cardiomyocytes and cardiomyocytes have first been demonstrated half a century ago where it

was shown that cardiac fibroblasts are able to synchronize electrical activity of adjacent cardiomyocytes in primary cell culture. [53] Recent studies in vitro showed that, apart from synchronizing electrical activity over appreciable distances,[54] cardiac myofibroblasts induce pro-arrhythmic slow conduction and ectopic activity following establishment of gap junctional coupling with cardiomyocytes.[55, 56] In combination, these two pillars of cardiac arrhythmogenesis were demonstrated to precipitate reentrant activity.[57] Generation of slow conduction and ectopic activity is based, as summarized schematically in Figure 8 Aa, on non-cardiomyocytes acting both as a resistive and a capacitive load on coupled cardiomyocytes:

(1) Coupled non-cardiomyocytes act as a resistive load: Cells of mesenchymal origin like fibroblasts have a modest membrane potential ($V_{m,non\text{-}CMC}$: -20 to –40 mV) compared to cardiomyocytes ($V_{m,CMC}$: -75 to -80 mV). Upon establishment of heterocellular gap junction coupling, the membrane potentials of the two cell types interact, with cardiomyocytes undergoing depolarization while non-cardiomyocytes undergo hyperpolarization. The degree to which the potentials equilibrate is dependent on the membrane resistance (r_m) of both cell types and the gap junctional resistance (r_{gj}), with the total difference in V_m dropping over the three resistors according to their relative sizes (cf. equation in Figure 8 Ab). [58]Thus, if the three resistances were identical, a V_m difference ($V_{m,non\text{-}CMC}$ - $V_{m,CMC}$) of 60 mV would cause the cardiomyocyte to depolarize by 20 mV and the fibroblast to hyperpolarize by 20 mV, while the remaining 20 millivolts would drop across the gap junctional resistance. In reality, changes in membrane potentials of the two cell types following gap junctional coupling are asymmetric because the specific membrane resistance of non-cardiomyocytes is typically larger than that of cardiomyocytes. For identically sized cells, this implies that r_m of non-cardiomyocytes substantially exceeds r_m of cardiomyocytes and that, for a heterologous cell pair, non-cardiomyocyte hyperpolarization accordingly outweighs cardiomyocyte depolarization. The consequences of cardiomyocyte depolarization by coupled non-cardiomyocytes are illustrated in Figure 8 B for the case of myofibroblasts being electrotonically coupled to cardiomyocytes forming a cell strand. With increasing density of coupled myofibroblasts, i.e., with increasing resistive load, V_m of cardiomyocytes gets increasingly depolarized (Figure 8 Bb). Conversely, conduction velocities show a biphasic change consisting of an initial increase followed by a decrease (Figure 8 Bc). This biphasic change (‘supernormal conduction’) is typical for cardiac tissue undergoing progressive depolarization and was being exposed to increasing concentrations of extracellular potassium. [38, 39, 59, 60] Further to inducing

pro-arrhythmic slow conduction, non-cardiomyocyte dependent cardiomyocyte depolarization is also responsible for the generation of ectopic activity because $V_{m,CMC}$ is reduced to levels where the sodium window current is operational (Figure 8C).

(2) Coupled non-cardiomyocytes act as a capacitive load: Apart from the size of the resistive load, impulse propagation velocity in cardiac tissue is dependent on the membrane capacitance of the tissue downstream of the excitation wavefront. At the single cell level, this can be understood by appreciating that it takes more time for an upstream cell to charge its downstream neighbor to threshold if the latter has a larger membrane capacitance. From studies in squid giant axons, conduction velocity was found to be inversely related to membrane capacitance. [61] Accordingly, even if the resting membrane potential of non-cardiomyocytes and cardiomyocytes were identical, electrotonic coupling between the two cell types would be expected to slow conduction as a function of capacitive load represented by then non-cardiomyocytes and the degree of gap junctional coupling.

In summary, electrotonic coupling of cardiomyocytes to non-excitable cells having a lesser membrane potential causes cardiomyocytes to undergo partial depolarization that leads to ectopic activity and conduction slowing due to increasing levels of sodium channel inactivation. Depolarization-dependent conduction slowing is further aggravated by the capacitive load exerted by coupled non-cardiomyocytes on neighboring cardiomyocytes that increases the time needed to reach threshold for sodium channel activation. While all of these pro-arrhythmic mechanisms are firmly established to be present in vitro, future studies are needed to show whether and to which extent these mechanisms are operational in intact cardiac tissue, and whether, apart from resident non-cardiomyocytes, the mechanisms outlined above may also contribute to pro-arrhythmic effects of stem cell therapies.[62]

LIMITATIONS OF EXPERIMENTAL MODELS AND PERSPECTIVE

Over the past years, experimental and theoretical work on cardiac impulse propagation has developed in two directions: (i) The use of models more closely replicating normal and diseased human hearts, and (ii) research based on findings of channel remodeling, regional diversity and cellular compartmentalization.

Discussions about the validity of given experimental models have been active for many decades. It is our opinion that work carried out in cell cultures using hearts of small rodents allow to define electrical and molecular change at very high resolution and are suited to establish *the principal biophysical rules* governing cardiac propagation. Indeed, the match between such experiments and computer simulations is striking. [7] However, computer simulations indicate that dimensionality plays a role in source-to-load mismatch insofar as the addition of a 3rd dimension increases the effect of the downstream load, and the interaction between ion current flow, cell-to-cell coupling and microstructure. [63]

A further point of discussion relates to the heterogeneity in distribution of gap junction plaques and ion channels contributing to depolarization, such as the Na^+ channel ($Na_v1.5$). Spach et al. [64] have shown that the fact that neonatal cardiomyocytes exhibit a rather uniform peripheral distribution of gap junction plaques as opposed to adult cardiomyocytes, where the majority plaques (~60%) is found at the cell ends [65] has little effect on propagation velocity. An open question still relates to the role of $Na_v1.5$ channels located in the intercalated disc in propagation. Experiments using genetically engineered ventricular and atrial mouse myocytes suggest that about 50% of $Na_v1.5$ channels are located in the intercalated disc, [66-70] whereby a fraction of these channels resides in close vicinity of gap junction plaques, the so-called perinexus. Early work by N. Sperelakis and more recent computer simulations [71-75] suggested that these channels may contribute the cell-to-cell transfer of cardiac impulses in presence of limited or in absence of cell-to-cell coupling by gap junctions. [76] Currently, experiments carried out at the cellular level are needed to provide an answer to this interesting hypothesis.

Finally, we have entered the area of stem cell research, which may allow to build 3-D cardiac tissue from myocytes induced pluripotent stem cells. Further development will be needed to use tissue engineered from an electrically homogeneous population of such cells for propagation studies.

REFERENCES

1. Mines GR. On dynamic equilibrium in the heart. *J Physiol*. 1913;46:349-83.
2. Pandit SV, Jalife J. Rotors and the dynamics of cardiac fibrillation. *Circ Res*. 2013;112:849-62.
3. Weidmann S. Electrical constants of trabecular muscle from mammalian heart. *J Physiol*. 1970;210:1041-54.
4. Rohr S, Kleber AG, Kucera JP. Optical recording of impulse propagation in designer cultures. Cardiac tissue architectures inducing ultra-slow conduction. *Trends Cardiovasc Med*. 1999;9:173-9.
5. Luo CH, Rudy Y. A model of the ventricular cardiac action potential. Depolarization, repolarization, and their interaction. *Circ Res*. 1991;68:1501-26.
6. Shaw RM, Rudy Y. Ionic mechanisms of propagation in cardiac tissue. Roles of the sodium and L-type calcium currents during reduced excitability and decreased gap junction coupling. *Circ Res*. 1997;81:727-41.
7. Kleber AG, Rudy Y. Basic mechanisms of cardiac impulse propagation and associated arrhythmias. *Physiol Rev*. 2004;84:431-88.
8. Delgado C, Steinhaus B, Delmar M, Chialvo DR, Jalife J. Directional differences in excitability and margin of safety for propagation in sheep ventricular epicardial muscle. *Circ Res*. 1990;67:97-110.
9. Kucera JP, Rudy Y. Mechanistic insights into very slow conduction in branching cardiac tissue: a model study. *Circ Res*. 2001;89:799-806.
10. Boyle PM, Vigmond EJ. An intuitive safety factor for cardiac propagation. *Biophys J*. 2010;98:L57-9.
11. Rohr S, Kucera JP, Kleber AG. Slow conduction in cardiac tissue, I: effects of a reduction of excitability versus a reduction of electrical coupling on microconduction. *Circ Res*. 1998;83:781-94.
12. Kleber AG, Janse MJ, Wilms-Schopmann FJ, Wilde AA, Coronel R. Changes in conduction velocity during acute ischemia in ventricular myocardium of the isolated porcine heart. *Circulation*. 1986;73:189-98.
13. Beauchamp P, Choby C, Desplantez T, de Peyer K, Green K, Yamada KA, Weingart R, Saffitz JE, Kleber AG. Electrical propagation in synthetic ventricular myocyte strands from germline connexin43 knockout mice. *Circ Res*. 2004;95:170-8.
14. Beauchamp P, Desplantez T, McCain ML, Li W, Asimaki A, Rigoli G, Parker KK, Saffitz JE, Kleber AG. Electrical Coupling and Propagation in Engineered Ventricular Myocardium With Heterogeneous Expression of Connexin43. *Circ Res*. 2012.
15. Joyner RW. Effects of the discrete pattern of electrical coupling on propagation through an electrical syncytium. *Circ Res*. 1982;50:192-200.
16. Joyner RW, van Capelle FJ. Propagation through electrically coupled cells. How a small SA node drives a large atrium. *Biophys J*. 1986;50:1157-64.
17. LeGrice IJ, Smaill BH, Chai LZ, Edgar SG, Gavin JB, Hunter PJ. Laminar structure of the heart: ventricular myocyte arrangement and connective tissue architecture in the dog. *Am J Physiol*. 1995;269:H571-82.
18. Pope AJ, Sands GB, Smaill BH, LeGrice IJ. Three-dimensional transmural organization of perimysial collagen in the heart. *Am J Physiol Heart Circ Physiol*. 2008;295:H1243-H1252.
19. Hooks DA, Trew ML, Caldwell BJ, Sands GB, LeGrice IJ, Smaill BH. Laminar arrangement of ventricular myocytes influences electrical behavior of the heart. *Circ Res*. 2007;101:e103-12.
20. Horn MA, Trafford AW. Aging and the cardiac collagen matrix: Novel mediators of fibrotic remodelling. *J Mol Cell Cardiol*. 2016;93:175-85.
21. Rutherford SL, Trew ML, Sands GB, LeGrice IJ, Smaill BH. High-resolution 3-dimensional reconstruction of the infarct border zone: impact of structural remodeling on electrical activation. *Circ Res*. 2012;111:301-11.
22. Spach MS, Miller WT, 3rd, Dolber PC, Kootsey JM, Sommer JR, Mosher CE, Jr. The functional role of structural complexities in the propagation of depolarization in the atrium of the dog. Cardiac conduction disturbances due to discontinuities of effective axial resistivity. *Circ Res*. 1982;50:175-91.
23. Spach MS, Kootsey JM. Relating the sodium current and conductance to the shape of transmembrane and extracellular potentials by simulation: effects of propagation boundaries. *IEEE Trans Biomed Eng*. 1985;32:743-55.
24. Spach MS, Dolber PC, Heidlage JF, Kootsey JM, Johnson EA. Propagating depolarization in anisotropic human and canine cardiac muscle: apparent directional differences in membrane capacitance. A simplified model for selective

directional effects of modifying the sodium conductance on Vmax, tau foot, and the propagation safety factor. *Circ Res*. 1987;60:206-19.
25. Spach MS, Heidlage JF. The stochastic nature of cardiac propagation at a microscopic level. Electrical description of myocardial architecture and its application to conduction. *Circ Res*. 1995;76:366-80.
26. Spach MS, Dolber PC, Heidlage JF. Influence of the passive anisotropic properties on directional differences in propagation following modification of the sodium conductance in human atrial muscle. A model of reentry based on anisotropic discontinuous propagation. *Circ Res*. 1988;62:811-32.
27. Cabo C, Pertsov AM, Baxter WT, Davidenko JM, Gray RA, Jalife J. Wave-front curvature as a cause of slow conduction and block in isolated cardiac muscle. *Circ Res*. 1994;75:1014-28.
28. Rohr S, Kucera JP. Involvement of the calcium inward current in cardiac impulse propagation: induction of unidirectional conduction block by nifedipine and reversal by Bay K 8644. *Biophys J*. 1997;72:754-66.
29. Wang Y, Rudy Y. Action potential propagation in inhomogeneous cardiac tissue: safety factor considerations and ionic mechanism. *Am J Physiol Heart Circ Physiol*. 2000;278:H1019-29.
30. Wilders R, Kumar R, Joyner RW, Jongsma HJ, Verheijck EE, Golod D, van Ginneken AC, Goolsby WN. Action potential conduction between a ventricular cell model and an isolated ventricular cell. *Biophys J*. 1996;70:281-95.
31. Joyner RW, Kumar R, Wilders R, Jongsma HJ, Verheijck EE, Golod DA, Van Ginneken AC, Wagner MB, Goolsby WN. Modulating L-type calcium current affects discontinuous cardiac action potential conduction. *Biophys J*. 1996;71:237-45.
32. Huelsing DJ, Pollard AE, Spitzer KW. Transient outward current modulates discontinuous conduction in rabbit ventricular cell pairs. *Cardiovasc Res*. 2001;49:779-89.
33. Fast VG, Kleber AG. Cardiac tissue geometry as a determinant of unidirectional conduction block: assessment of microscopic excitation spread by optical mapping in patterned cell cultures and in a computer model. *Cardiovasc Res*. 1995;29:697-707.
34. Rohr S, Kucera JP, Fast VG, Kleber AG. Paradoxical improvement of impulse conduction in cardiac tissue by partial cellular uncoupling. *Science*. 1997;275:841-4.
35. Kucera JP, Kleber AG, Rohr S. Slow conduction in cardiac tissue, II: effects of branching tissue geometry. *Circ Res*. 1998;83:795-805.
36. Janse MJ, Kleber AG. Electrophysiological changes and ventricular arrhythmias in the early phase of regional myocardial ischemia. *Circ Res*. 1981;49:1069-81.
37. Gettes LS, Reuter H. Slow recovery from inactivation of inward currents in mammalian myocardial fibres. *J Physiol*. 1974;240:703-24.
38. Spear JF, Moore EN. Supernormal excitability and conduction in the His-Purkinje system of the dog. *Circ Res*. 1974;35:782-92.
39. Spear JF, Moore EN. Effect of potassium on supernormal conduction in the bundle branch-Purkinje system of the dog. *Am J Cardiol*. 1977;40:923-8.
40. Kondratyev AA, Ponard JG, Munteanu A, Rohr S, Kucera JP. Dynamic changes of cardiac conduction during rapid pacing. *Am J Physiol Heart Circ Physiol*. 2007;292:H1796-811.
41. Kleber AG, Riegger CB, Janse MJ. Electrical uncoupling and increase of extracellular resistance after induction of ischemia in isolated, arterially perfused rabbit papillary muscle. *Circ Res*. 1987;61:271-9.
42. Thibodeau IL, Xu J, Li Q, Liu G, Lam K, Veinot JP, Birnie DH, Jones DL, Krahn AD, Lemery R, Nicholson BJ, Gollob MH. Paradigm of genetic mosaicism and lone atrial fibrillation: physiological characterization of a connexin 43-deletion mutant identified from atrial tissue. *Circulation*. 2010;122:236-44.
43. Boulaksil M, Winckels SK, Engelen MA, Stein M, van Veen TA, Jansen JA, Linnenbank AC, Bierhuizen MF, Groenewegen WA, van Oosterhout MF, Kirkels JH, de Jonge N, Varro A, Vos MA, de Bakker JM, van Rijen HV. Heterogeneous Connexin43 distribution in heart failure is associated with dispersed conduction and enhanced susceptibility to ventricular arrhythmias. *Eur J Heart Fail*. 2010;12:913-21.
44. Kitamura H, Ohnishi Y, Yoshida A, Okajima K, Azumi H, Ishida A, Galeano EJ, Kubo S, Hayashi Y, Itoh H, Yokoyama M. Heterogeneous loss of connexin43 protein in nonischemic dilated cardiomyopathy with ventricular tachycardia. *J Cardiovasc Electrophysiol*. 2002;13:865-70.

45. Gutstein DE, Morley GE, Vaidya D, Liu F, Chen FL, Stuhlmann H, Fishman GI. Heterogeneous expression of Gap junction channels in the heart leads to conduction defects and ventricular dysfunction. *Circulation*. 2001;104:1194-9.
46. Prudat Y, Kucera JP. Nonlinear behaviour of conduction and block in cardiac tissue with heterogeneous expression of connexin 43. *J Mol Cell Cardiol*. 2014;76:46-54.
47. Jalife J. Rotors and spiral waves in atrial fibrillation. *J Cardiovasc Electrophysiol*. 2003;14:776-80.
48. Jalife J. Inward rectifier potassium channels control rotor frequency in ventricular fibrillation. *Heart Rhythm*. 2009;6:S44-8.
49. Munoz V, Grzeda KR, Desplantez T, Pandit SV, Mironov S, Taffet SM, Rohr S, Kleber AG, Jalife J. Adenoviral expression of IKs contributes to wavebreak and fibrillatory conduction in neonatal rat ventricular cardiomyocyte monolayers. *Circ Res*. 2007;101:475-83.
50. Sun Y, Kiani MF, Postlethwaite AE, Weber KT. Infarct scar as living tissue. *Basic research in cardiology*. 2002;97:343-7.
51. Quinn TA, Camelliti P, Rog-Zielinska EA, Siedlecka U, Poggioli T, O'Toole ET, Knopfel T, Kohl P. Electrotonic coupling of excitable and nonexcitable cells in the heart revealed by optogenetics. *Proc Natl Acad Sci U S A*. 2016;113:14852-14857.
52. Lefroy DC, Fang JC, Stevenson LW, Hartley LH, Friedman PL, Stevenson WG. Recipient-to-donor atrioatrial conduction after orthotopic heart transplantation: surface electrocardiographic features and estimated prevalence. *Am J Cardiol*. 1998;82:444-50.
53. Hyde A, Blondel B, Matter A, Cheneval JP, Filloux B, Girardier L. Homo- and heterocellular junctions in cell cultures: an electrophysiological and morphological study. *Progress in brain research*. 1969;31:283-311.
54. Gaudesius G, Miragoli M, Thomas SP, Rohr S. Coupling of cardiac electrical activity over extended distances by fibroblasts of cardiac origin. *Circ Res*. 2003;93:421-8.
55. Miragoli M, Gaudesius G, Rohr S. Electrotonic modulation of cardiac impulse conduction by myofibroblasts. *Circ Res*. 2006;98:801-10.
56. Miragoli M, Salvarani N, Rohr S. Myofibroblasts induce ectopic activity in cardiac tissue. *Circ Res*. 2007;101:755-8.
57. Zlochiver S, Munoz V, Vikstrom KL, Taffet SM, Berenfeld O, Jalife J. Electrotonic myofibroblast-to-myocyte coupling increases propensity to reentrant arrhythmias in two-dimensional cardiac monolayers. *Biophys J*. 2008;95:4469-80.
58. Salvarani N, Maguy A, De Simone SA, Miragoli M, Jousset F, Rohr S. TGF-beta1 (Transforming Growth Factor-beta1) Plays a Pivotal Role in Cardiac Myofibroblast Arrhythmogenicity. *Circ Arrhythm Electrophysiol*. 2017;10:e004567.
59. Dominguez G, Fozzard HA. Influence of extracellular K+ concentration on cable properties and excitability of sheep cardiac Purkinje fibers. *Circ Res*. 1970;26:565-74.
60. Kagiyama Y, Hill JL, Gettes LS. Interaction of acidosis and increased extracellular potassium on action potential characteristics and conduction in guinea pig ventricular muscle. *Circ Res*. 1982;51:614-23.
61. Matsumoto G, Tasaki I. A study of conduction velocity in nonmyelinated nerve fibers. *Biophys J*. 1977;20:1-13.
62. Macia E, Boyden PA. Stem cell therapy is proarrhythmic. *Circulation*. 2009;119:1814-23.
63. Fast VG, Kleber AG. Block of impulse propagation at an abrupt tissue expansion: evaluation of the critical strand diameter in 2- and 3-dimensional computer models. *Cardiovasc Res*. 1995;30:449-59.
64. Spach MS, Heidlage JF, Dolber PC, Barr RC. Electrophysiological effects of remodeling cardiac gap junctions and cell size: experimental and model studies of normal cardiac growth. *Circ Res*. 2000;86:302-11.
65. Hoyt RH, Cohen ML, Saffitz JE. Distribution and three-dimensional structure of intercellular junctions in canine myocardium. *Circ Res*. 1989;64:563-574.
66. Desplantez T, McCain ML, Beauchamp P, Rigoli G, Rothen-Rutishauser B, Parker KK, Kleber AG. Connexin43 ablation in foetal atrial myocytes decreases electrical coupling, partner connexins, and sodium current. *Cardiovasc Res*. 2012;94:58-65.
67. Milstein ML, Musa H, Balbuena DP, Anumonwo JM, Auerbach DS, Furspan PB, Hou L, Hu B, Schumacher SM, Vaidyanathan R, Martens JR, Jalife J. Dynamic reciprocity of sodium and potassium channel expression in a macromolecular complex controls cardiac excitability and arrhythmia. *Proc Natl Acad Sci U S A*. 2012.
68. Petitprez S, Zmoos AF, Ogrodnik J, Balse E, Raad N, El-Haou S, Albesa M, Bittihn P, Luther S, Lehnart SE, Hatem SN, Coulombe A, Abriel H. SAP97 and dystrophin macromolecular complexes determine two pools of cardiac sodium channels Nav1.5 in cardiomyocytes. *Circ Res*. 2011;108:294-304.

69. Sato PY, Musa H, Coombs W, Guerrero-Serna G, Patino GA, Taffet SM, Isom LL, Delmar M. Loss of plakophilin-2 expression leads to decreased sodium current and slower conduction velocity in cultured cardiac myocytes. *Circ Res*. 2009;105:523-6.
70. Cerrone M, Noorman M, Lin X, Chkourko H, Liang FX, van der Nagel R, Hund T, Birchmeier W, Mohler P, van Veen TA, van Rijen HV, Delmar M. Sodium Current Deficit and Arrhythmogenesis in a Murine Model of Plakophilin-2 Haploinsufficiency. *Cardiovasc Res*. 2012.
71. Sperelakis N. Lack of electrical coupling between contiguous myocardial cells in vertebrate hearts. *Experientia Suppl*. 1969;15:135-65.
72. Tarr M, Sperelakis N. Weak Electrotonic Interaction between Contiguous Cardiac Cells. *Am J Physiol*. 1964;207:691-700.
73. Kucera JP, Rohr S, Rudy Y. Localization of sodium channels in intercalated disks modulates cardiac conduction. *Circ Res*. 2002;91:1176-82.
74. Mori Y, Fishman GI, Peskin CS. Ephaptic conduction in a cardiac strand model with 3D electrodiffusion. *Proc Natl Acad Sci U S A*. 2008;105:6463-8.
75. Veeraraghavan R, Lin J, Hoeker GS, Keener JP, Gourdie RG, Poelzing S. Sodium channels in the Cx43 gap junction perinexus may constitute a cardiac ephapse: an experimental and modeling study. *Pflugers Arch*. 2015;467:2093-105.
76. Rhett JM, Ongstad EL, Jourdan J, Gourdie RG. Cx43 associates with Na(v)1.5 in the cardiomyocyte perinexus. *J Membr Biol*. 2012;245:411-22.

FIGURES AND LEGENDS

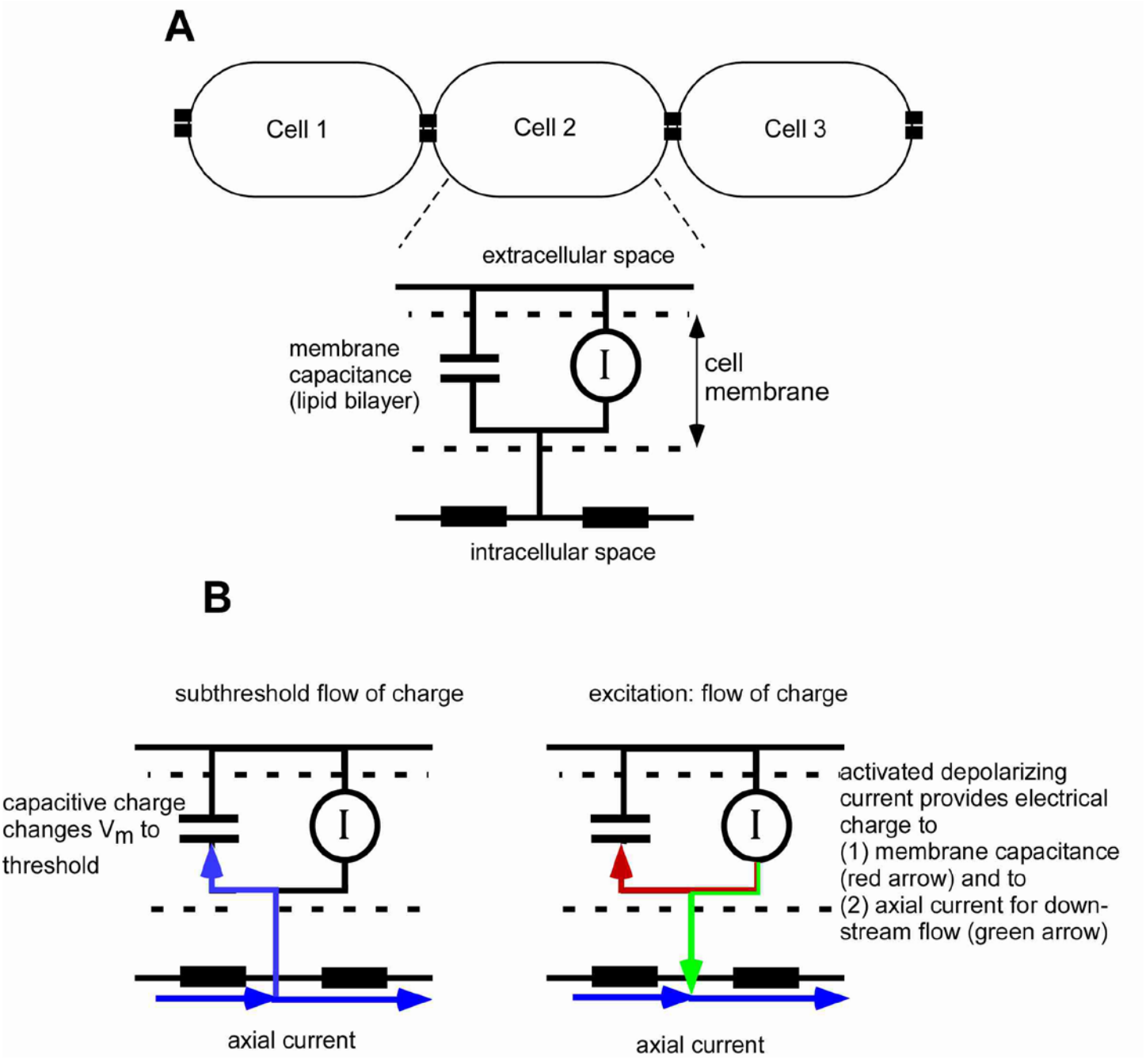

Figure 1: **Model of a cardiac cell chain used to model cardiac propagation**. Panel A: Single cell chain; cells separated by resistors representing gap junction channels (top), and excitable elements (equivalent circuit) formed by a capacitor representing the lipid bilayer and a current generator (I) representing the lumped ion channels and exchangers in the membrane (bottom).
Panel B: With the wavefront approaching the cellular element, part of the axial current (blue) flows into the element and depolarizes the membrane to threshold for activation of Na^+ and/or Ca^{2+} channels (left). Once activated, depolarizing inward current (red) initiates the action potential by delivering charge to the membrane capacitance and delivers axial current for excitation of downstream cells.

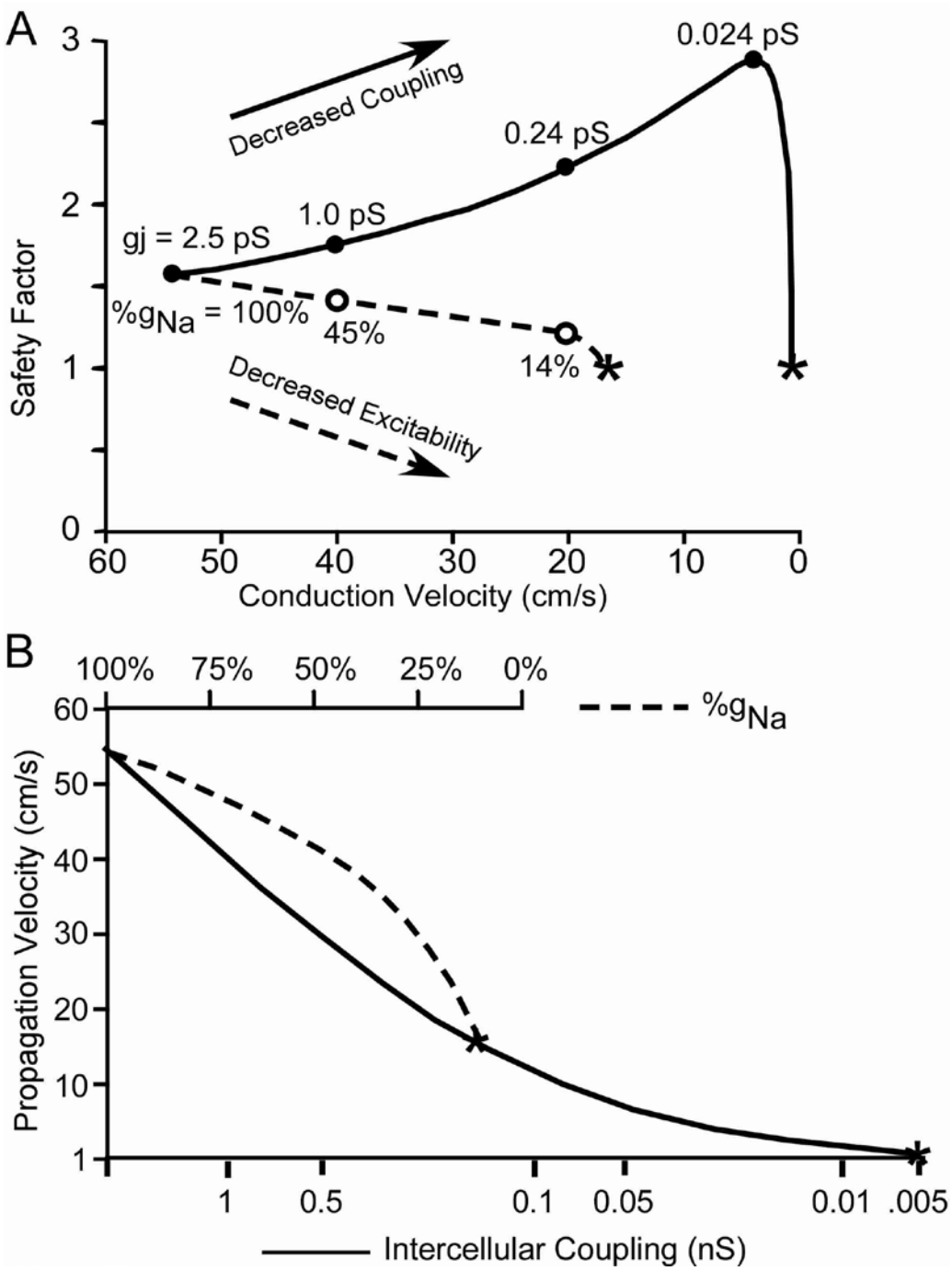

Figure 2: **Effect of Na^+ channel inhibition and cell-to-cell uncoupling on the safety factor (SF) and velocity of electrical propagation (computer model of a cell chain)**. Panel A: Decrease of cell-to-cell coupling conductance (g_j) and inhibition of Na^+ channel conductance (g_{Na}) have opposite effects on SF Reduction of g_{Na} causes a monotonic decrease of SF with conduction block occurring at approximately 85% inhibition. Cell-to-cell uncoupling renders propagation safer with propagation block occurring only *beyond* an > 100-fold decrease of g_j.
Panel B: Na^+ channel inhibition causes a continuous decrease in propagation velocity and abrupt block at a relatively high velocity (15 cm/s at 85% inhibition). By contrast propagation block develops only beyond a 100-fold decrease of g_j, at velocities in the order of 1 cm/s. Note the logarithmic scale of the abscissa for g_j. From reference [6] with permission.

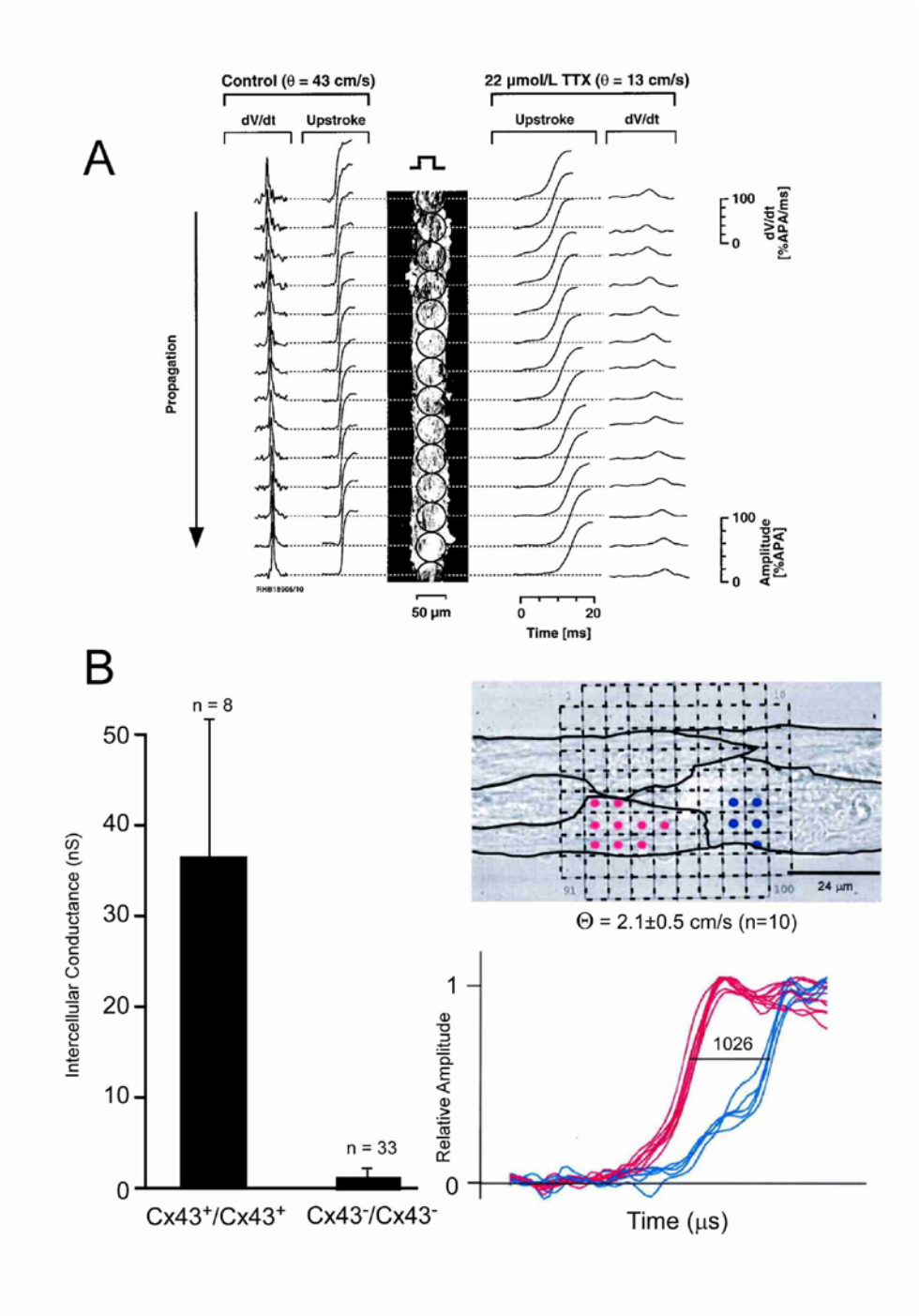

Figure 3: **Effect of Na^+ channel inhibition and cell-to-cell uncoupling on safety factor and velocity of electrical propagation (experimental work)** Panel A: Engineered strand of neonatal rat ventricular myocytes. Action potential upstrokes are measured by a voltage-sensitive dye. Left side : rapid action potential upstrokes during normal propagation at a velocity of 43 cm/s. Right side: I_{Na} inhibition (tetrodotoxin): Upstrokes carried by the L-type Ca^{2+} currents are slow, propagation velocity, Θ, has decreased to 13cm/s.
Panel B: Left hand graph: column plots depicting the intercellular conductance, g_j, in pairs of fetal murine ventricular myocytes. Genetic ablation of Cx43 produces a > 90% decrease of g_j. Right hand panel: strand of fetal murine ventricular myocytes engineered from $Cx43^-/Cx43^-$ cells. The cell from which the cluster of action potential upstrokes represented in blue were recorded was excited 1026 µs after the previous upstream cell (red upstrokes). This "saltatory" type of propagation produces a very slow propagation velocity of 2.1 cm/s. Reproduced with permission from references [11, 13] .

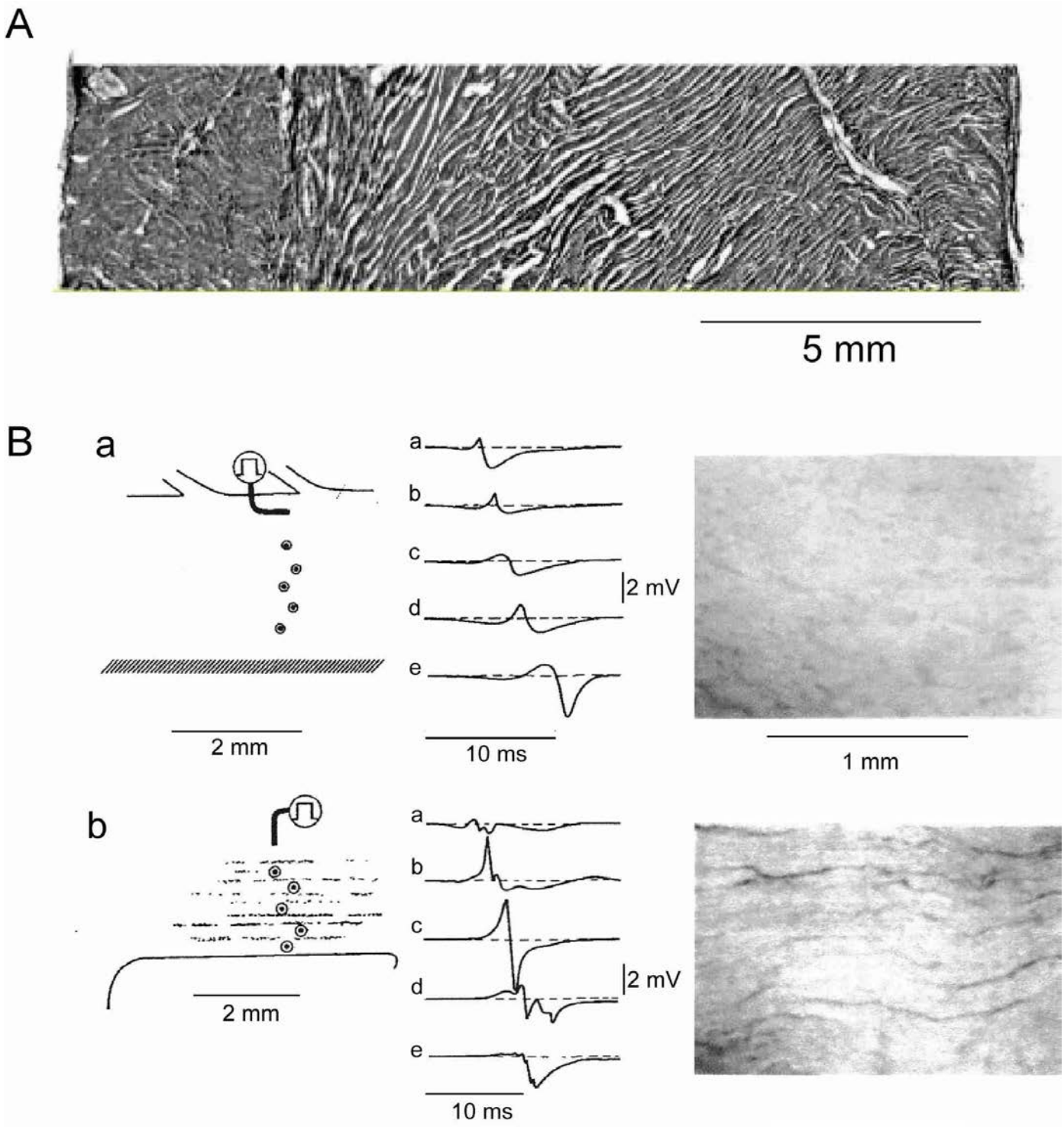

Figure 4: Panel A: Transmural section across the left ventricular wall of a pig heart showing laminar architecture (modified from reference [19] with permission). Panel B: Propagation in canine atrial trabecula with continuous structure (Ba, young dog) versus discontinuous structure (Bb, aged dog). The structural differences are visualized in the histological sections (right) showing the presence of fine fibrous septa between the longitudinally oriented cardiac fibers. The extracellular electrograms in panel Ba are of a smooth shape with a single instrinsic deflection, typical for a homogeneous wavefront. The electrograms in Bb are fractionated, indicating heterogeneous transverse impulse spread. Slightly modified from reference [22] with permission.

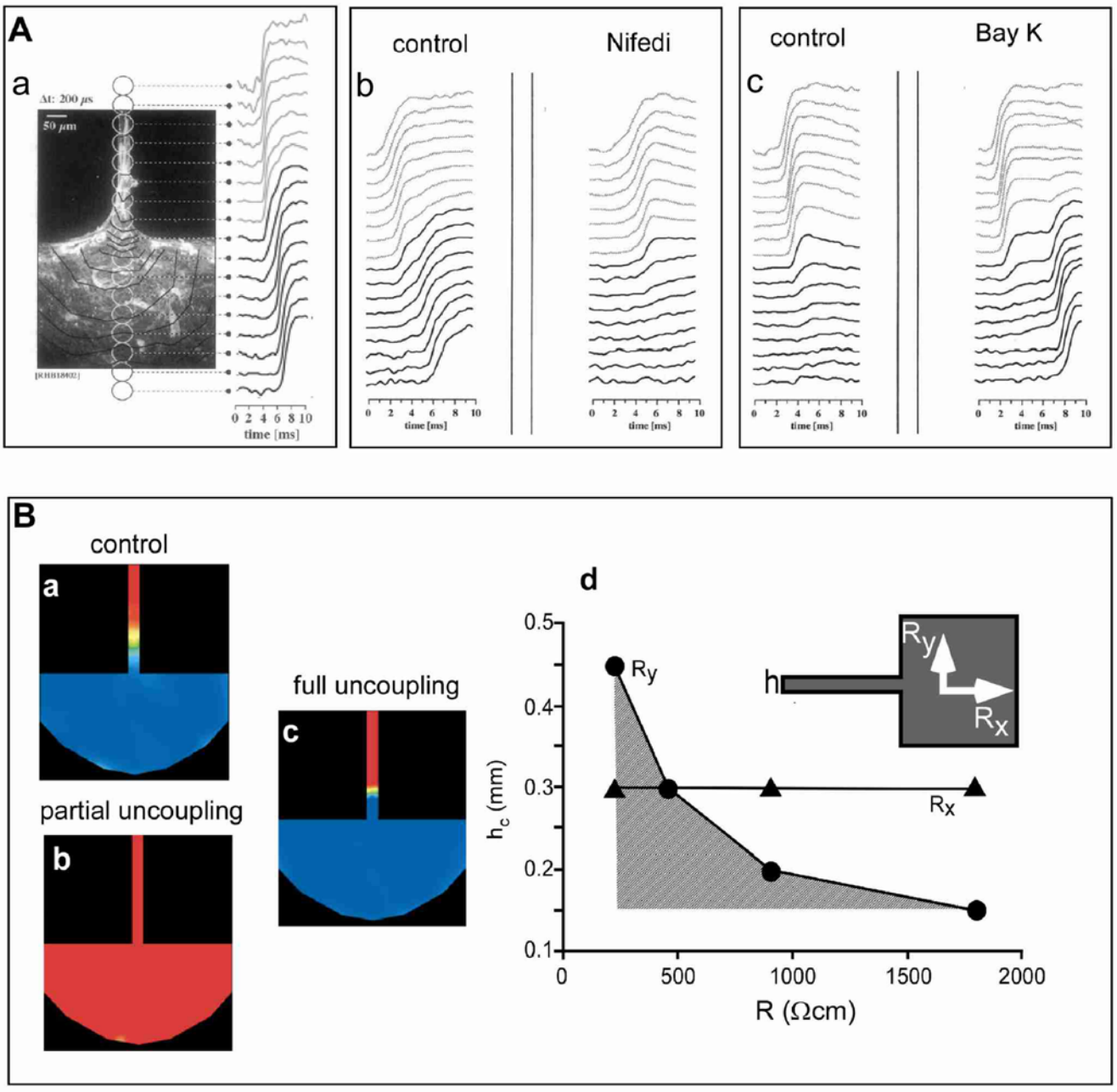

Figure 5: Panel A: Left, Aa: Source-to-sink mismatch at a transition from a small bundle to a large bulk of tissue in a patterned culture of neonatal rat ventricular myocytes. Middle, Ab: Forward propagation from a narrow strand to the bulk tissue produces a local propagation delay >2ms. Nifedipine, an inhibitor of $I_{Ca,L}$ blocks propagation across at the transition. Right, Ac: Complete block at the transition due to source-to-sink mismatch under control conditions (strand <50μm in width). Enhancement of $I_{Ca,L}$ with Bay K 8644 restores anterograde propagation. Panel B: Effect of partial cell-to-cell uncoupling at a site of source-to-sink mismatch. Ba: Source-to-sink mismatch produces block at the transition of a narrow cell strand (≤ 50 μm) to the bulk tissue (red: excited tissue; blue: non-excited tissue). Bb: Partial uncoupling by local superfusion with palmitoleic acid restores propagation across the expansion. Bc: Full local uncoupling causes conduction block. Bd: Graph from computer simulations showing that restoring propagation depends on the increase of cell-to-cell resistance transverse to the main axis of the strand, while changes in the longitudinal resistance do not affect block formation (h_c = width of the strand at which block occurs). Reproduced and modified with permission from references [28, 33, 34].

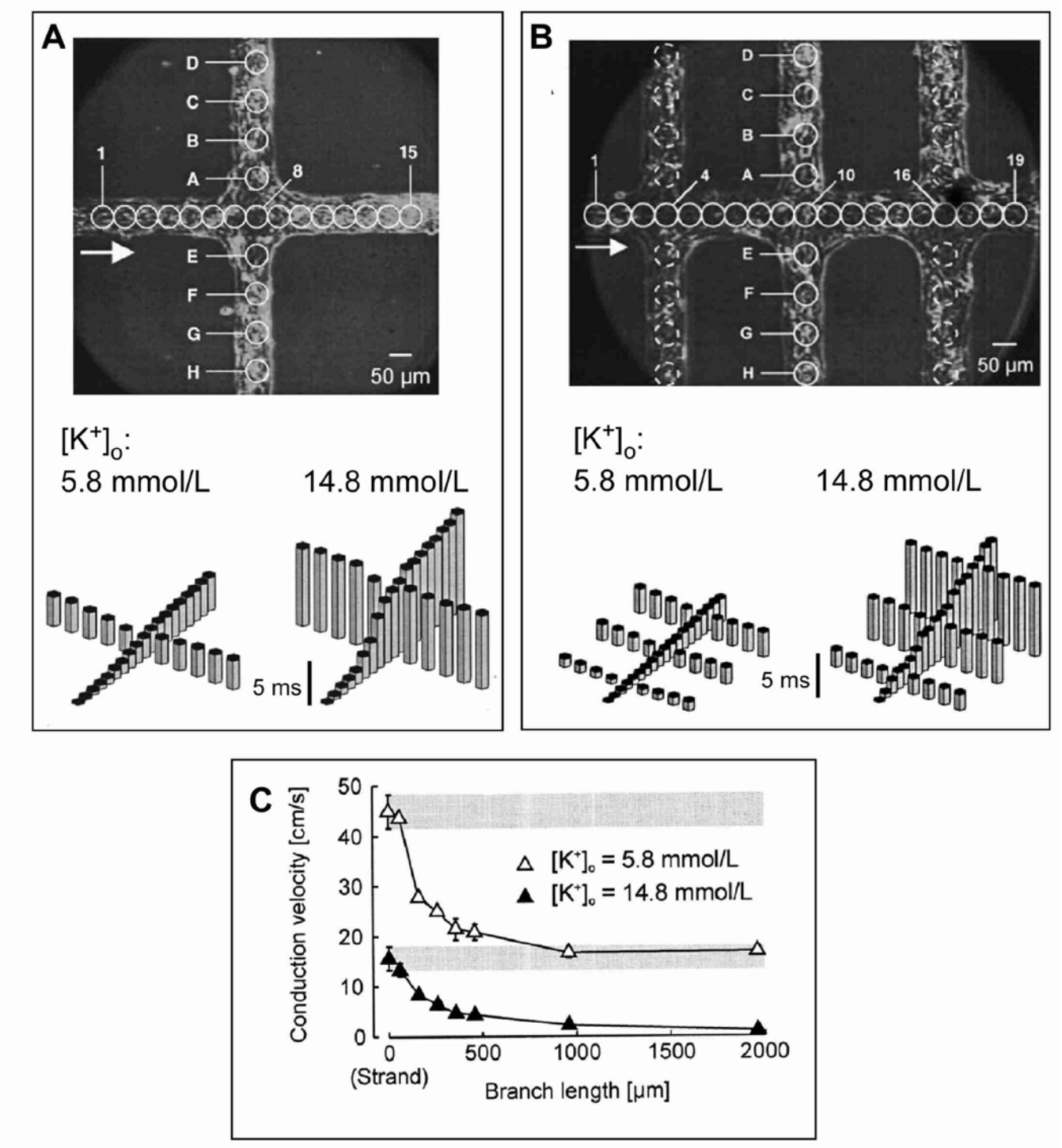

Figure 6: Propagation in branching tissue. Panel A: Propagation in a strand (horizontal) releasing two branches (vertical). The structure is illustrated on top together with superimposed white circles corresponding to the location of photodiodes used to optically record transmembrane voltage changes. Lower graphs show activation times in milliseconds as columns. As excitation approaches the branching point, propagation slows down (visualized by the steeper profile of activation times). This effect is enhanced in presence of 14.8 mmol/L extracellular K^+, a condition which inactivates I_{Na}. Panel B: Repetitive branching slowing propagation. Panel C. Dependence of average propagation velocity in the main strand on the length of the side branches. The current sink (or "pull" effect) increases up to a length of about 1 mm. From reference [35] with permission.

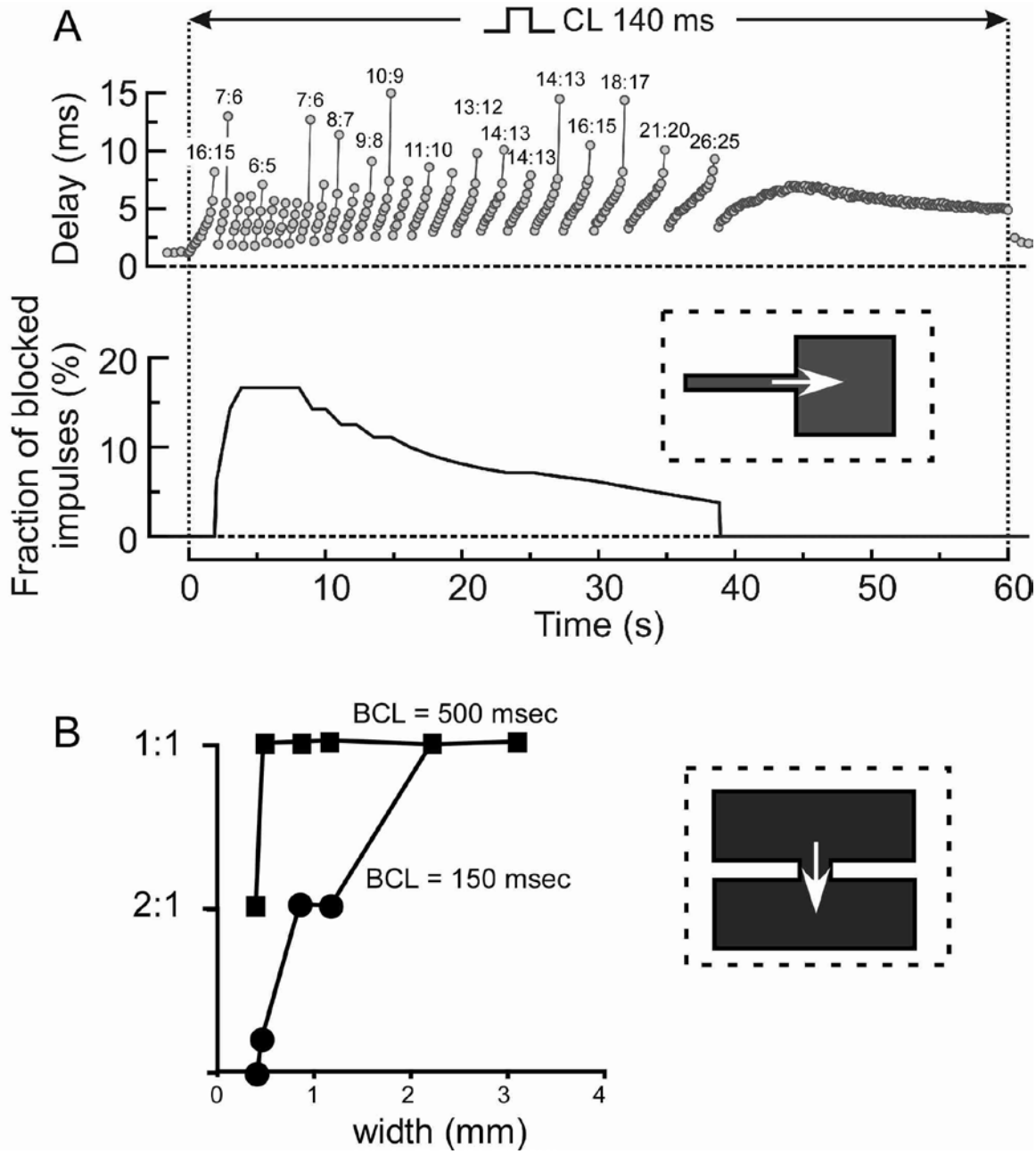

Figure 7: **Effect of heterogeneous tissue structure on frequency-dependence of propagation**. Panel A: Propagation across a tissue expansion in cultured neonatal rat ventricular myocytes. Shown is the effect of a change in basis cycle length (BCL) upon a decrease from a steady-state value of 500 ms to 140 ms for 60 s (arrows). Top: With rapid stimulation at a BCL of 140 ms, conduction delays increase monotonically until block occurs after the 15th impulse. The time associated with block permits partial recovery of the tissue in the expansion and, accordingly, the next activation produces a relatively short delay. Subsequently, conduction delays get prolonged again and block occurs after 6 beats. This pattern repeats itself until about 40 seconds, when propagation is completely restored. The lower graph shows the degree of block expressed as a fraction of the conducted beats. Panel B: Graph taken from experiments in which a narrow isthmus was cut into an epicardial slice taken from of a sheep ventricle. Propagation gets blocked to a variable degree, depending on the width of the isthmus. At a BCL of 500 ms propagation is blocked every second beat at an isthmus width <0.5 mm, and 1:1 propagation is observed at isthmuses > 0.5 mm in width. Stimulation at 150 ms BCL leads to a much stronger dependence of conduction on microstructure with establishment of 1:1 propagation only at an isthmus width > 2mm. From references [27] and [40] with permission.

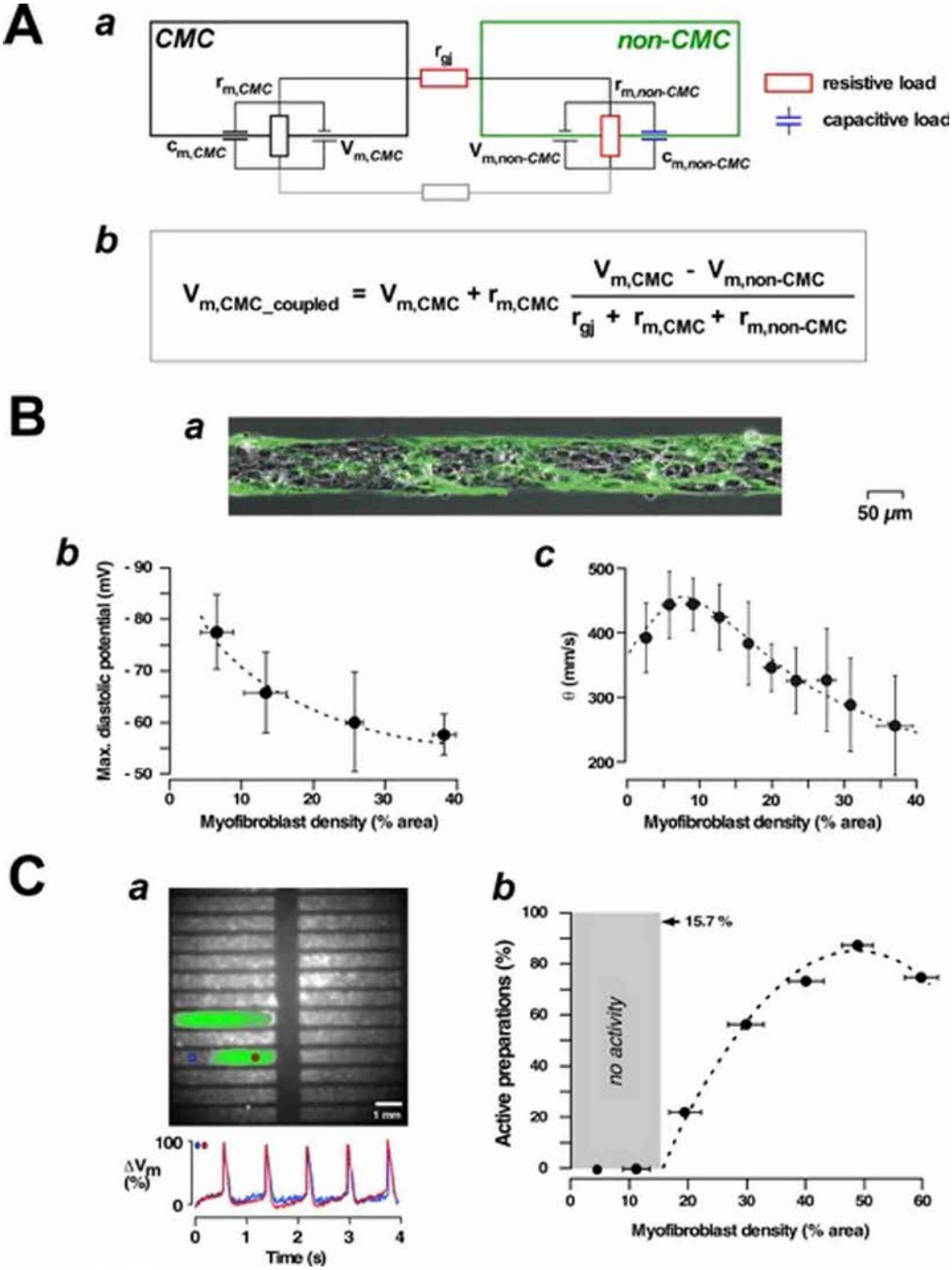

Figure 8: Pro-arrhythmic effects of non-cardiomyocytes coupled to cardiomyocytes. A. Resistive and capacitive loading effects: (a) Schematic of the resistive and capacitive components of the load exerted by non-cardiomyocytes (non-CMCs) on coupled cardiomyocytes (CMCs); r_m: membrane resistance, r_{gj}: gap junctional resistance; c_m: membrane capacitance (b) Equation describing the effect of non-cardiomyocytes on the resting membrane potential of coupled cardiomyocytes. B. Effects of non-CMCs coupled to CMCs on impulse conduction: (a) preparation consisting of a strand of cardiomyocytes coated with myofibroblasts (green: α-smooth muscle staining). (b) Myofibroblast-density dependent decrease of the resting potential of coupled CMCs. (c) Myofibroblast-induced biphasic change of conduction velocity. Adapted from[55]. C. Induction of ectopic activity by myofibroblasts coupled to cardiomyocytes: (a) Image of the experimental preparation consisting of multiple strands of cardiomyocytes coated with myofibroblasts with green areas indicating ongoing ectopic activity. Action potentials recorded optically at sites indicated in one strand (blue and red dots) are shown below. (b) Spontaneous activity of strand preparation as function of the density of coating myofibroblasts. Adapted from[56].